

Structure of Aluminum Films for the Creation of Tunnel Junctions¹

M. V. Strelkov^{a, b, *}, A. M. Chekushkin^a, A. A. Lomov^c, S. V. Kraevskii^d,
M. Yu. Fominskii^a, and M. A. Tarasov^a

^a Institute of Radioengineering and Electronics, Russian Academy of Sciences, Moscow, 125009 Russia

^b Moscow Institute of Physics and Technology (National Research University), Dolgoprudny, Moscow oblast, 141701 Russia

^c Physicotechnological Institute, Russian Academy of Sciences, Moscow, 117218 Russia

^d Research Institute of Biomedical Chemistry, Moscow, 119121 Russia

*e-mail: strelkov.mv@phystech.edu

Received May 17, 2023; revised August 1, 2023; accepted August 3, 2023

Abstract—A series of studies of the structure of aluminum films deposited on single-crystal silicon substrates in different temperature regimes has been carried out. The roughness and grain size of 20-nm thick films of nuclei deposited at elevated temperatures and also dusted over the nucleus layer at room temperature to a thickness of 150 nm was studied using an atomic force microscope. The film profile was measured in an electron microscope. It is found that films on a hot sublayer turn out to be smoother, more rigid (less friable), and make it possible to expect the creation of superconductor–insulator–superconductor and superconductor–insulator–normal metal transitions with a higher current density and lower capacitance, respectively.

DOI: 10.1134/S1064226923100157

INTRODUCTION

The actually achieved parameters of Josephson tunnel junctions turn out to be much worse than the theoretical estimates, so for niobium SQUIDs with a tunnel barrier made of aluminum oxide, characteristic voltage $V_c = I_c R_n$ at best, reaches 200 μ V, and according to theory it should be up to 2 mV. For terahertz mixers and generators based on superconductor–insulator–superconductor (SIS) junctions, the main problems are a large specific capacitance, hysteresis, and the appearance of leakage currents. Both problems can be associated with the morphology and crystal structure of the tunnel barrier films and superconducting electrodes. In practice, the films are granular, the tunnel barriers are uneven, and the effective area is at the level of 10%, hence the leaks and parasitic capacitances. The crystal structure determines fundamentally different properties of the same elements, such as diamond, graphite, fullerenes, and carbon nanotubes. The key elements of a promising superconducting technology are the use of single-crystal substrates matched in lattice constant and orientation with the grown films, optimization of growth temperature conditions, and controlled formation of an oxide or nitride tunnel barrier.

1. MANUFACTURING AND STRUCTURE ANALYSIS

In this study, aluminum films were grown by magnetron sputtering on a Si(111) substrate with a quasi-

epitaxial seed layer. The films were deposited in two stages, by analogy with [1]. First, an island layer of 10–20 nm of single-crystal nuclei was formed on the substrate for 100 s at a temperature of 400°C, deposition rate of Al particles was not more than 0.2 nm/s, pressure in the chamber was 1.5×10^{-3} mbar and magnetron power was 300 W. The sample cooling process up to 19°C passed under conditions of residual pressure for 12 h. Film deposition at the second stage was carried out under conditions of a stationary temperature of the sample. The film deposition process took place in an argon atmosphere (pressure 4×10^{-3} mbar) at a speed of 1.45 nm/s for 138 s. The temperature of the silicon substrate was fixed at 19°C due to controlled cooling of the substrate table from a water-cooling apparatus (chiller). The image of the layers and films deposited on top of the nuclei obtained with an atomic force microscope (AFM) is shown in Figs. 1 and 2, respectively. The measurement data for the graininess of the layers and films deposited on top of the nuclei are given in Tables 1 and 2, respectively. Separately, prepared embryonic films up to 20 nm thick and films with two-stage aluminum deposition were studied. The cross section of a film with a quasi-epitaxial sublayer is shown in Fig. 3. X-ray diffraction measurements can be used to determine the crystallographic structure of the films and the orientation of the crystal lattice, the orientation being predominantly (111). The diffraction patterns are shown in Figs. 4. The mechanical properties of the grown Al/Si (111) films were also measured on a CB-500 Nanovea (United States) setup using a nanoindenter, which was

¹ The work was awarded a prize at the 19th Ivan Anisimkin Young Scientists Competition.

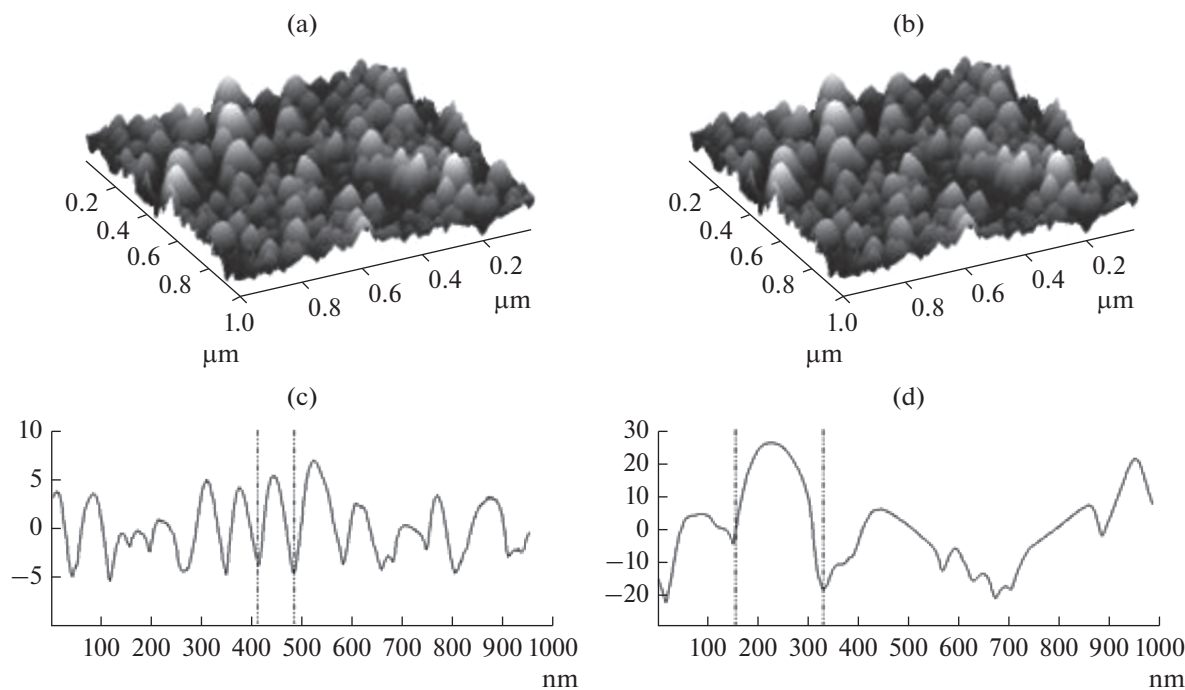


Fig. 1. AFM images of a 20-nm film of a nucleation film deposited on a hot substrate (a) and a substrate at room temperature (b), profiles of a nucleation film deposited on a hot substrate (c) and on a substrate at room temperature (d) obtained on an AFM microscope.

a Berkovich trihedral diamond pyramid with a radius of 50 nm. Direct and inverse dependences of the applied load on the depth of penetration of the indenter were obtained (mode of continuous measurement of stiffness). The average results are given in Table 3.

2. MEASUREMENT OF PARAMETERS

Aluminum samples were measured, identical in size and made in the form of strips 0.2 mm wide and

10 mm long. For film thicknesses of 2 nm or less, the electrical resistance was measured on the order of $1 \text{ M}\Omega$; the film, apparently, was an island: it consisted of weakly bonded regions. At a thickness of 6 nm, the resistivity was $\rho = 2 \times 10^{-6} \text{ Ohm m}$, at a thickness of 20 nm, $\rho = 2.9 \times 10^{-7} \text{ Ohm m}$. The resistance of films with a thickness of more than 300 nm approached the tabular value for bulk aluminum, $\rho = 2.6 \times 10^{-8} \text{ Ohm m}$. At small thicknesses, the film consists of conductive islands separated by weakly conductive gaps, and as the thickness increases, the conductive regions merge.

Table 1. Characteristics of the films depending on the temperature of the substrate at which the layer was deposited

$T_h, ^\circ\text{C}$	Grain size, nm	Roughness, nm	
		peak to peak	rms
200	160	25	6.6
400	60	10	1.6
500	70	5	0.8

Table 2. Parameters of a 150-nm film depending on the nucleus deposition temperature T_{dep}

$T_{\text{dep}}, ^\circ\text{C}$	Grain size, nm	Roughness, nm	
		peak to peak	rms
400	200	20	7
Room	300–400	25–40	8–25

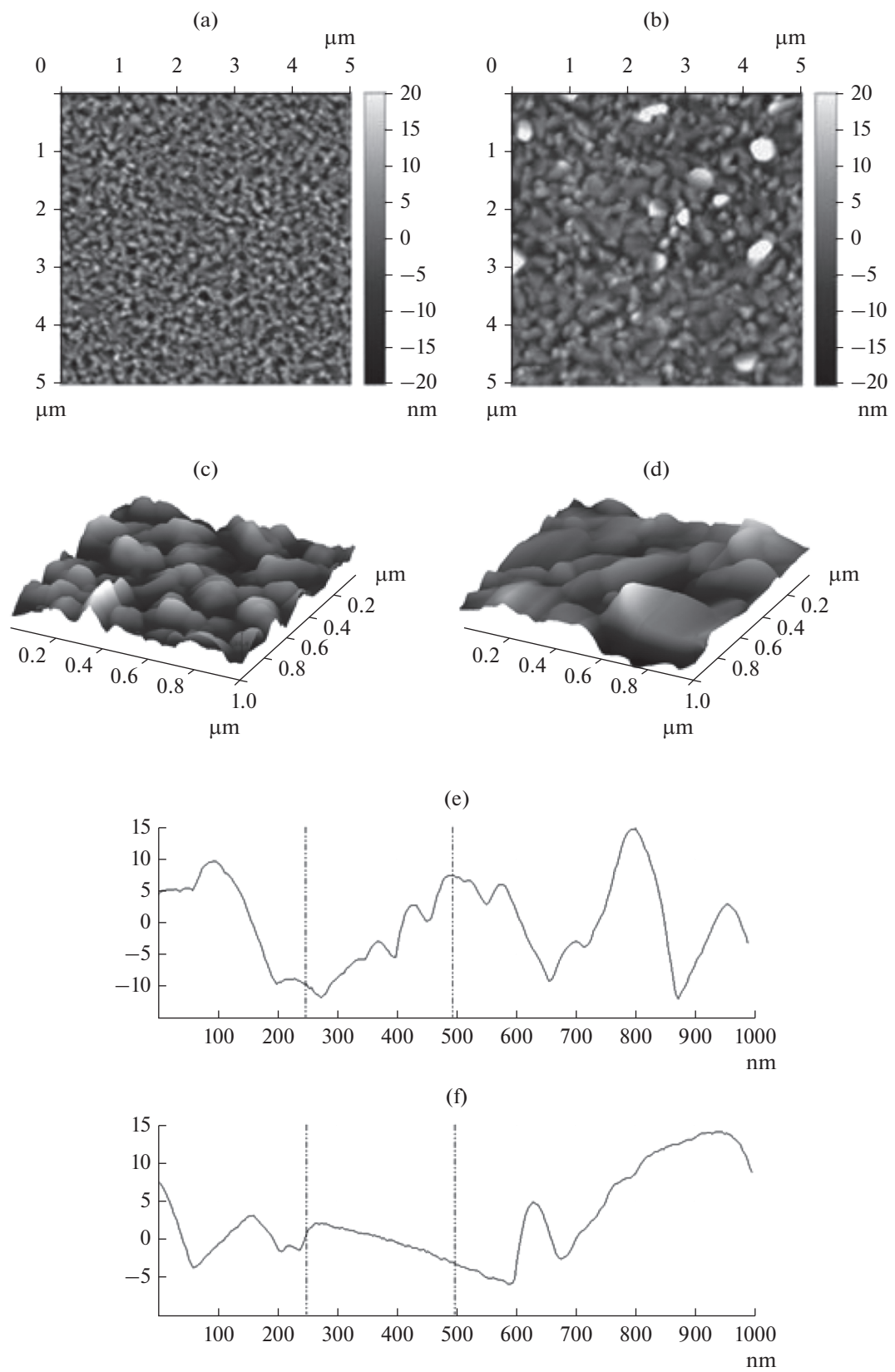


Fig. 2. 150 nm films deposited over a "hot" nucleus 20 nm thick (a, c) and on a substrate at room temperature (b, d), profiles of films deposited over a "hot" nucleus (e) and over a substrate at room temperature (f).

Table 3. Film hardness depending on growth conditions

Conditions	Hardness, GPa	Young's modulus, GPa
Cold sublayer	5.5	40
Hot undercoat	16	95
Reference 200 nm	5	35

The low conductivity of amorphous thin films can be due to the localization of charge carriers on weakly bound clusters and the scattering of electrons by defects. The critical temperature of the superconducting transition of films 18 and 3 nm thick is 1.5 and 2.4 K, respectively.

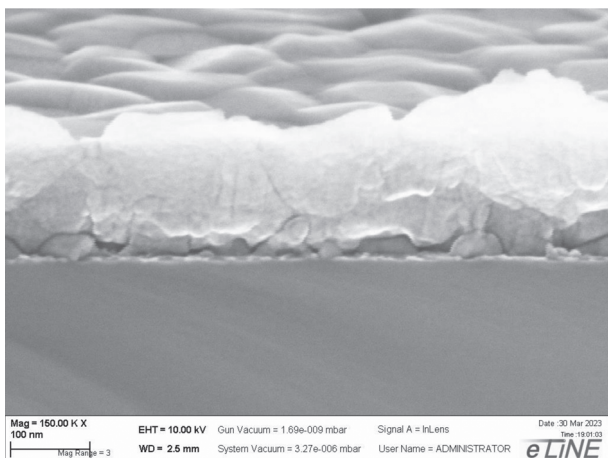


Fig. 3. Image of a cleavage in an electron microscope: a granular layer nucleus with a thickness of about 20 nm is clearly visible from below (screenshot).

The parameters of SIS tunnel junctions are largely determined by the structure of the aluminum oxide or aluminum nitride barrier region. For practical tunnel junctions with a resistance of 1 to 2 k Ω / μm^2 specific capacitance measured from resonances is from 70 to 50 fF/ μm^2 . According to the formula for a flat capacitor $C = \epsilon\epsilon_0 S/d$, where $\epsilon_0 = 8.85 \times 10^{-12}$ f/m and $\epsilon = 3$, this corresponds to the thickness of the oxide barrier $d = \epsilon\epsilon_0 S/C = 0.38\text{--}0.5$ nm. For a tunnel junction at these resistances, the estimated barrier thickness is approximately 1.8 nm, for an ideal flat capacitor this would correspond to a specific capacitance of 15 fF/ μm^2 , i.e., the difference in thickness estimation in theory is 4.7–3.6 times, so the capacitance is formed over a larger area than the effective area of the tunnel barrier. In reality, the relative permittivity of even an ideal amorphous barrier turns out to be less than two; the effective thickness of the capacitive barrier will be at the level of 0.25 nm. It can be assumed that the rough surface has a much larger area with lower transparency. According to [2], the effective tunneling area is 0.13. This means that only a small (thinner) part of the junction area is responsible for tunneling conduction, while the rest (thicker part) determines the effective parasitic capacitance. However, it is rather difficult to rely on an ideal tunneling barrier, since for AlO_x the actual measured lattice con-

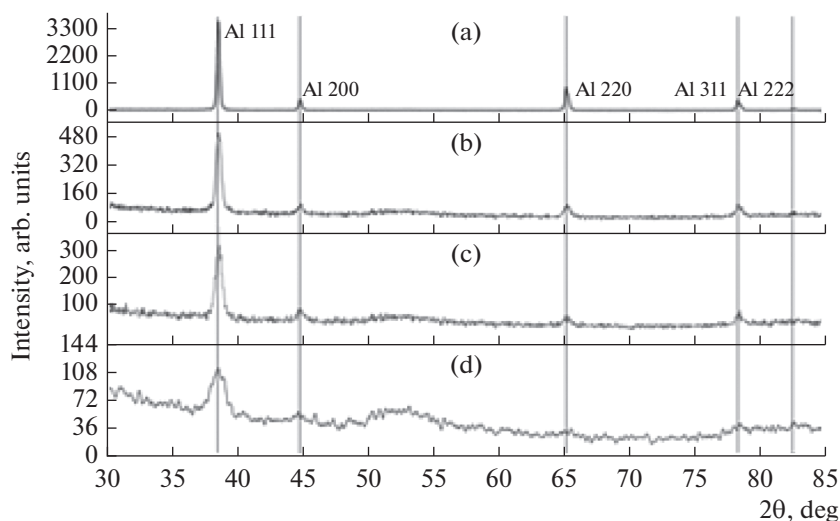


Fig. 4. X-ray diffraction patterns of films 200 (a), 20 (b, c) and 10 nm (d) thick, deposited at high (a, b) and low (c, d) speeds; All films exhibit a peak corresponding to the (111) substrate orientation: (a) 200 nm, high deposition rate; (b) 20 nm, high rate; (c) 20 nm, low rate; (d) 10 nm, low rate.

Table 4. Theoretical estimates of the parameters of aluminum films

Al thickness, nm	J_c , $\mu\text{A}/\mu\text{m}^2$	R_n , $\text{Ohm}/\mu\text{m}^2$	V_c , μV	C , $\text{fF}/\mu\text{m}^2$	β_c	$\tau = RC$, ps	$f_{RC} = 1/2\pi\tau$, THz
1	36	5.6	196	24	0.014	0.13	1

stant is 0.47 nm; an ideal junction would be a tunnel barrier with a thickness approximately equal to the dielectric lattice constant. This requires the formation of an atomically smooth crystalline surface without defects and twins. In this case, the junction area will be an order of magnitude smaller than the standard junctions on granular films at the same values of tunneling conductance.

Table 4 shows theoretical estimates for tunnel junctions with an area of $1 \mu\text{m}^2$ with a dielectric thickness of 1 and 2 nm in SIS junctions based on aluminum films.

CONCLUSIONS

The creation of epitaxial atomically smooth superconducting tunnel junctions will make it possible to get rid of hysteresis and the need for resistive shunting of junctions (or reduce their influence), which means a significant improvement in all limiting characteristics for devices of superconducting analog and digital electronics.

FUNDING

This study was supported financially by the Russian Science Foundation (project no. 23-79-00022). Unique scientific installations Cryointegral and Avogadro were used, the work on which was financially supported by the Ministry of Science and Higher Education of the Russian Federation (agreement no. 075-15-2021-667 and agreement no. 075-15-2021-933, respectively).

CONFLICT OF INTEREST

The authors declare that they do not have any conflicts of interest.

REFERENCES

1. I. Rodionov, A. Baburin, A. Gabidullin, et al., *Sci. Rep.* **9**, 12232 (2019).
2. T. Greibe, M. Stenberg, C. Wilson, et al., *Phys. Rev. Lett.* **106**, 097001 (2011).

SPELL: 1. ok